Mechanics of Composite Materials, Vol. 59, No. 5, November, 2023

IMPACT OF THE SHEAR AND THICKNESS STRETCHING EFFECTS ON THE FREE VIBRATIONS OF ADVANCED COMPOSITE PLATES

A. Messaoudi,[1,2] A. Bouhadra,[3,4*] A. Menasria,[3,4] B. Mamen,[3,4] B. Boucham,[1] M. Benguediab,[1] A. Tounsi,[4,5,6,7] and M. A. Al-Osta[6,7]

Keywords: *advanced composite plates, dimensionality effect, thickness stretching, free vibration, Hamilton's principle, Navier's solution.*

Quasi-3D high-order shear deformation theories (HSDT) are often more effective for investigating advanced composite thick plates than two-dimensional (2D) theories. The present study examines the specific dimensionality effect of quasi-3D HSDT theories through-thickness stretching on the free vibration behavior of thin-thick rectangular plates. For this purpose, a 3D displacement field defined by only five unknowns is proposed. Besides, it contains a stretching component that contributes to the whole behavior of the plate. The results of the 2D model are compared to the results of the quasi-3D model. In addition, several factors, such as the aspect ratio, geometrical ratio, and material index, illustrate the influence of dimensionality. Young's modulus and densities should be graded in the direction of thickness. The motion equations are deduced based on Hamilton's *principle. According to the boundary condition type, Navier's solution method is used for solving the obtained equations. The results show that the inclusion of the stretching component would increase the dynamic response of the thick advanced composite plates. Moreover, the influence of dimensionality is less significant for pure ceramic plates.*

[1]Department of mechanical Engineering, University of Sidi Bel Abbes, Faculty of Technology, Algeria
[2]University of Abbès Laghrour Khenchela, Faculty of Sciences and Technology, Mechanic Engineering Department, Algeria
[3]University of Abbès Laghrour Khenchela, Faculty of Sciences and Technology, Civil Engineering Department, Algeria
[4]Materials and Hydrology Laboratory, University of Sidi Bel Abbes, Faculty of Technology, Civil Engineering Department, Algeria
[5]YFL (Yonsei Frontier Lab), Yonsei University, Seoul, Korea
[6]Department of Civil and Environmental Engineering, King Fahd University of Petroleum & Minerals, 31261 Dhahran, Eastern Province, Saudi Arabia
[7]Interdisciplinary Research Center for Construction and Building Materials, KFUPM, Dhahran, Saudi Arabia
[*]Corresponding author; e-mail: bouhadrahako@gmail.com

Original article submitted July 15, 2022; revision submitted February 28, 2023.

1. Introduction

Recently, a new class of advanced composites functionally graded materials (FGMs) has received special attention. Following their advantageous characteristics with high strength-to-weight and stiffness-to-weight ratios, they were successfully utilized in nuclear engineering, the aerospace industry, and high-temperature conditions, unlike traditional composite materials [1]. Although these materials are intended for aerospace and aeronautics, they have found their place in other fields such as automotive, biomedical, military defense, electrical, electronics, thermoelectric, athletes, etc. [2-6].

In general, FGMs are composed of a mixture of ceramic and metal. Many researchers are interested in studying the free vibration and dynamic behavior, bending, and buckling response of FGM beams, shells, and plates [7-15]. They spend time understanding the mechanical behavior of FGMs, which enables to design an optimal profile.

FGM plates can be analyzed using many theories, such as the classical plate theory (CPT). Arshid et al. [16] studied the free vibration analysis of a circular plate composed of a porous material with integrated piezoelectric actuator patches using Hamilton's variational principle and the CPT to obtain the governing motion equations for various boundary conditions. Using the isogeometric analysis based on CPT, Valizadeh et al. [17] numerically studied the buckling of free and forced vibration analyses of orthotropic plates. Many researchers used CPT to obtain the problem solutions [18-21]. Using the first-order shear deformation theory (FSDT) and the finite element method (FEM), Zghal et al. [22] investigated the large deflection behavior of nanocomposite structures, having geometrical nonlinearity and reinforced with carbon nanotubes [23-26]. Recently, Zhou and Zhu [27] analyzed the vibration and wave problems of composites reinforced by graphene platelets (GPLs), considering four types of dispersions along the z -direction, using FSDT. Bourihane et al. [28] examined the nonlinear dynamic of functionally graded (FG) plates subjected to external dynamic loading using the third-order shear deformation theory (TSDT) implicit algorithm to solve stationary nonlinear problems and structural nonlinear dynamic problems. Zhou et al. [29] using TSDT studied the bending and vibrations of thin-thick FG rectangular plates with simply supported edges submitted to a magneto-electric field. Several investigations using the higher-order shear deformation theory (HSDT) with nonlinear variations of displacements in the thickness of the plate, such as TSDT, were carried out [30-32]. Shahsavari et al. [33] considered a novel quasi-3D hyperbolic theory to study the free vibration analysis of FG porous plates with the Winkler/Kerr/Pasternak foundations. Arefi et al. [34] developed a theory with sinusoidal shear deformation theory (SSDT) for investigating the elastic bending analysis of FG polymer composite plate reinforced with graphene platelets resting on Pasternak foundation. Many researchers used SSDT in their solutions [35-36].

Zigzag theories (ZZT) are also utilized in [37-39]. The quasi-3D approach considering a normal stretching influence was also used in [40-42]. However, some of these theories are computationally expensive due to the number of additional variables included in the model. CPT and FSDT are the most widely accepted and applied approaches for determining stresses and strains in the plates as simpler and more computationally efficient theories. The influence of shear deformation by means of a linear variation of the plane displacements through the thickness are considered in the FSDT by applying a correction factor. To improve the representation of transverse shear stresses without correction factors, HSDT theories were developed in order to overcome the drawbacks of CPT and FSDT. These theories include higher-order terms in approximating the in-plane displacement fields and satisfying the zero shear stress conditions at the outer sides of the plates.

Several analytical and numerical models were applied to study the mechanical and dynamic response of advanced composite materials and nanostructures. Yaylacı et al. [43] using finite element ANSYS and ABAQUS software studied the receding contact problem of elastic layer and elastic quarter plane. Yaylacı et al. [44] analyzed the continuous and discontinuous receding contact problems between FG layer and rigid foundation using analytical solutions and FEM. Öner et al. [45] employing FEM and an artificial neural network (ANN) studied the contact problem of multilayer FGM structures under uniformly distributed compressive traction. Pourabdy et al. [46] analyzed the dynamic behavior of FG circular nanoplates using the nonlocal strain gradient (NSG) model. Daikh et al. [47] studied the equilibrium of FGM sandwich nanoplates using a novel nonlocal theory. Bouhadra et al. [48] using the Eringen theory analyze the stability behavior of imperfect FG nanobeam under mechanical loading.

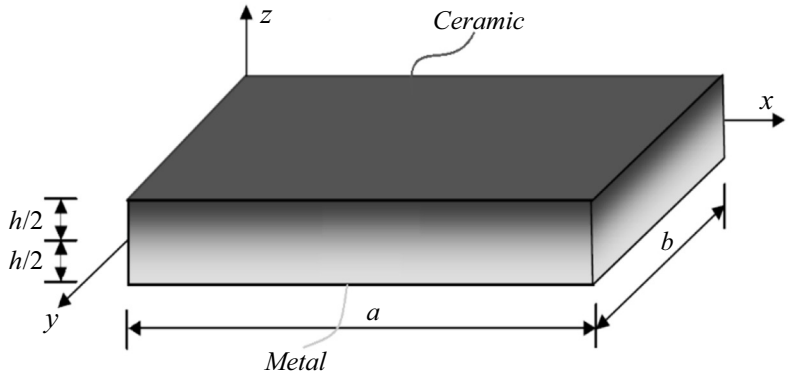

Fig. 1. A schematic of FG plate in the Cartesian coordinates system.

The free vibration response of the square FGM advanced composite plates with simply supported edges was studied to estimate the specific dimensional effect through-thickness stretching using a hybrid function shape and quasi-3D HSDT. Only five unknowns included in the selected displacement field and the transverse shear effect was taken into account. The transverse displacements over the plate thickness satisfy the stress-free boundary conditions. The power-law scheme distribution shows that mechanical properties vary continuously with plate thickness. In addition, the five motion equations generated are also developed using Hamilton's principle and solved applying the Navier's approach for simply supported boundary conditions.

The main objective of this study is to use a new displacement field containing fewer unknowns compared to other quasi-3D shear deformation theories. This model simplifies the problem and considers the effect of transverse stretching, which is not considered in the case of 2D shear deformation theories. However, the boundary conditions are the main limitation of the present model compared to computational methods. In other words, the present model could be only used for simply supported plates. However, with a slight modification in solutions, the present model could effectively predict the behavior of clamped or simply clamped FG plates.

In addition, a more comprehensive analysis studied the effect of many parameters on natural frequencies, including the side-to-thickness ratio, thickness ratio, aspect ratio, volume fraction index, and material properties. Finally, numerical results were verified by comparisons with other theory solutions for plates found in the literature to ensure the accuracy and effectiveness of the theory proposed. It was concluded that the specific dimensional effect of quasi-3D HSDT theory significantly affects the free vibrations of the FG advanced composite plates. Therefore, the resulting negative implications of stretching thickness are reduced by implementing suitable quasi-3D theories.

2. Theoretical Formulations

2.1. Material proprieties and geometrical configuration of FG plate

Figure 1 shows the plate with uniform thickness h, length a, and width b. The Cartesian coordinate system x, y, z has the midplane plane $z = 0$.

The volume fraction of the FG rectangular plates is considered to follow a function with a power-law change along the z-direction:

$$V_c = \left(\frac{1}{2} + \frac{z}{h} \right)^k . \tag{1}$$

The actual material properties such as Young's modulus E and material density ρ are expressed based on the rule of mixtures as follows:

$$P(z) = (P_c - P_m)V + P_m, \tag{2}$$

where P is the property of the material for the FG plate; P_1 and P_2 will represent the properties of the top and bottom faces, respectively.

2.2. Kinematics

Based on HSDT and taking into account the impact of normal and transverse stresses (thickness-stretching), the plate displacement field can be expressed as:

$$\begin{aligned} u(x,y,z,t) &= u_0(x,y,t) - zw_{0,x} + k_1 f(z)\int \theta(x,y,t)\,dx, \\ v(x,y,z,t) &= v_0(x,y,t) - zw_{0,y} + k_2 f(z)\int \theta(x,y,t)\,dy, \\ w(x,y,z,t) &= w_0(x,y,t) + g(z)\varphi_z(x,y,t), \end{aligned} \tag{3}$$

where

$$k_1 = \alpha^2, \quad k_2 = \beta^2. \tag{4}$$

The following assumptions are considered.

The displacements are small compared to the plate thickness; therefore, the strains involved are infinitesimal.

The transverse displacement $\boldsymbol{w}$ includes two components: bending (w_0) and stretching effect (φ_z).

The displacements u in the x-direction and v in the y-direction consist of extension, bending, and shear components.

The function shape can be found as [13]:

$$f(z) = \left[\ln(\pi \exp(\frac{1}{20})) - (0.1407)^{(\frac{5}{6})} \cosh(\pi z) \right] z, \tag{5}$$

where

$$g(z) = r\left(\frac{df(z)}{dz}\right). \tag{6}$$

Note that the coefficient r can take two values:

$$\text{if} \begin{cases} r = 0, \ \text{2D case}, \\ r = 1, \ \text{3D case}. \end{cases} \tag{7}$$

Hereafter, we consider only the 3D case. 2D case can be obtained by considering the value $r = 0$.

The strain functions can be given by:

$$\begin{Bmatrix} \varepsilon_x \\ \varepsilon_y \\ \gamma_{xy} \end{Bmatrix} = \begin{Bmatrix} \varepsilon_x^0 \\ \varepsilon_y^0 \\ \gamma_{xy}^0 \end{Bmatrix} + z\begin{Bmatrix} k_x^b \\ k_y^b \\ k_{xy}^b \end{Bmatrix} + f(z)\begin{Bmatrix} k_x^s \\ k_y^s \\ k_{xy}^s \end{Bmatrix}, \quad \begin{Bmatrix} \gamma_{yz} \\ \gamma_{xz} \end{Bmatrix} = g(z)\begin{Bmatrix} \gamma_{yz}^0 \\ \gamma_{xz}^0 \end{Bmatrix}, \quad \varepsilon_z = g'(z)\,\varepsilon_z^0, \tag{8}$$

where

$$\begin{Bmatrix} \varepsilon_x^0 \\ \varepsilon_y^0 \\ \gamma_{xy}^0 \end{Bmatrix} = \begin{Bmatrix} u_{0,x} \\ v_{0,y} \\ u_{0,y} + v_{0,x} \end{Bmatrix}, \quad \begin{Bmatrix} k_x^b \\ k_y^b \\ k_{xy}^b \end{Bmatrix} = \begin{Bmatrix} -w_{0,xx} \\ -w_{0,yy} \\ -2w_{0,xy} \end{Bmatrix}, \tag{9}$$

$$\begin{Bmatrix} k_x^s \\ k_y^s \\ k_{xy}^s \end{Bmatrix} = \begin{Bmatrix} k_1\theta \\ k_2\theta \\ k_1\dfrac{\partial}{\partial y}\int \theta\, dx + k_2\dfrac{\partial}{\partial x}\int \theta\, dy \end{Bmatrix}, \quad \begin{Bmatrix} \gamma_{yz}^0 \\ \gamma_{xz}^0 \end{Bmatrix} = \begin{Bmatrix} k_2\int \theta\, dy + \varphi_{z,y} \\ k_1\int \theta\, dx + \varphi_{z,x} \end{Bmatrix}, \quad \varepsilon_z^0 = \varphi_z . \tag{10}$$

The integral terms that are employed in Eq. (10) should be determined by a Navier's method and are given as follows:

$$\frac{\partial}{\partial y}\int \theta\, dx = A'\theta_{,xy}, \ \frac{\partial}{\partial x}\int \theta\, dy = B'\theta_{,xy}, \ \int \theta\, dx = A'\theta_{,x}, \ \int \theta\, dy = B'\theta_{,y}, \tag{11}$$

where the coefficients A' and B' are expressed according to the type of solution used; in this case, it is via Navier's solution.

Therefore, A', B', k_1 and k_2 are expressed as follows:

$$A' = -\frac{1}{\alpha^2}, \quad B' = -\frac{1}{\beta^2}, \quad k_1 = \alpha^2, \quad k_2 = \beta^2, \tag{12}$$

where α and β are used in Eq. (29).

2.3. Constitutive relations

The linear constitutive relations of an FG plate in the case of the 3D formulation can be expressed as:

$$\sigma_{ij} = 2\mu(z)\varepsilon_{ij} + \lambda(z)\varepsilon_{kk}\delta_{ij} . \tag{13}$$

The coefficients μ and λ in terms of engineering constants are given below:

$$\lambda(z) = \frac{E(z)}{(1-2\nu)(1+\nu)}, \qquad \mu(z) = \frac{E(z)}{2(1+\nu)}. \tag{14}$$

2.4. Motion equations

This study uses Hamilton's principle to derive the motion equations. The principle can be expressed in analytical form as follows:

$$0 = \int_0^T (\delta U - \delta K)dt , \tag{15}$$

where δU is the strain energy variation, δK is the kinetic energy variation. The strain energy variation of the plate is determined by:

$$\begin{aligned} \delta U &= \int_{-h/2}^{h/2}\int_A [\sigma_x\delta\varepsilon_x + \sigma_y\delta\varepsilon_y + \sigma_z\delta\varepsilon_z + \tau_{xy}\delta\gamma_{xy} + \tau_{yz}\delta\gamma_{yz} + \tau_{xz}\delta\gamma_{xz}]dAdz \\ &= \int_A [N_x\delta\varepsilon_x^0 + N_y\delta\varepsilon_y^0 + N_z\delta\varepsilon_z^0 + N_{xy}\delta\gamma_{xy}^0 + M_x^b\delta k_x^b + M_y^b\delta k_y^b \\ &+ M_{xy}^b\delta k_{xy}^b + M_x^s\delta k_x^s + M_y^s\delta k_y^s + M_{xy}^s\delta k_{xy}^s + S_{yz}^S\delta\gamma_{yz} + S_{xz}^S\delta\gamma_{xz}]dA = \mathbf{0}, \end{aligned} \tag{16}$$

in which: A represents the surface. N, M, and Q are the resultants of stresses. Stiffness components are expressed as:

$$\begin{Bmatrix} N_x & N_y & N_{xy} \\ M_x^b & M_y^b & M_{xy}^b \\ M_x^s & M_y^s & M_{xy}^s \end{Bmatrix} = \int_{-h/2}^{h/2} (\sigma_x, \sigma_y, \tau_{xy}) \begin{Bmatrix} 1 \\ z \\ f(z) \end{Bmatrix} dz,$$

$$N_z = \int_{-h/2}^{h/2} \sigma_z \, g'(z) \, dz \,, \quad (S_{xz}^s, S_{yz}^s) = \int_{-h/2}^{h/2} (\tau_{xz}, \tau_{yz}) \, g(z) \, dz \,. \tag{17}$$

The kinetic energy variation of the plate can be written as:

$$\delta K = \int_{-h/2}^{h/2} \int_A [\frac{\partial u}{\partial t} \frac{\partial (\delta u)}{\partial t} + \frac{\partial v}{\partial t} \frac{\partial (\delta v)}{\partial t} + \frac{\partial w}{\partial t} \frac{\partial (\delta w)}{\partial t}] \, \rho(z) dA \, dz$$

$$= \int_A \{ I_0 [\dot{u}_0 \delta \dot{u}_0 + \dot{v}_0 \delta \dot{v}_0 + \dot{w}_0 \delta \dot{w}_0]$$

$$- I_1 [\dot{u}_0 \delta \dot{w}_{0,x} + \dot{v}_0 \delta \dot{w}_{0,y} + \dot{w}_{0,x} \delta \dot{u}_0 + \dot{w}_{0,y} \delta \dot{v}_0] + I_2 [\dot{w}_{0,x} \delta \dot{w}_{0,x} + \dot{w}_{0,y} \delta \dot{w}_{0,y}]$$

$$- J_1 [\dot{u}_0 \delta \dot{\theta}_{,x} + \dot{\theta}_{,x} \delta \dot{u}_0 + \dot{v}_0 \delta \dot{\theta}_{,y} + \dot{\theta}_{,y} \delta \dot{v}_0] + J_2 [\dot{w}_{0,x} \delta \dot{\theta}_{,x} + \dot{\theta}_{,x} \delta \dot{w}_{0,x} + \dot{w}_{0,y} \delta \dot{\theta}_{,y}$$

$$+ \dot{\theta}_{,y} \delta \dot{w}_{0,y}] + K_2 [\dot{\theta}_{,x} \delta \dot{\theta}_{,x} + \dot{\theta}_{,y} \delta \dot{\theta}_{,y}] + J_1^s [\dot{w}_0 \delta \dot{\varphi}_z + \dot{\varphi}_z \delta \dot{w}_0] + K_2^s \dot{\varphi}_z \delta \dot{\varphi}_z \} dA, \tag{18}$$

in which dot-superscript convention designates the differential with regard to the time variable t and $(I_0, I_1, J_1, J_1^s, I_2, J_2, K_2, K_2^s)$ are the mass inertias that can be determined as follows:

$$(I_0, I_1, J_1, J_1^s, I_2, J_2, K_2, K_2^s) = \int_{-h/2}^{h/2} (1, z, f, g, z^2, zf, f^2, g^2) \rho(z) dz \,. \tag{19}$$

Putting the terms of δU, δK, and δV from Eqs. (16) and (18) into Eq. (15), then, integrating and collecting the common coefficients of $\delta u_0, \delta v_0, \delta w_0, \delta \theta,$ and δf_z, the motion equations of the plate can be determined as follows:

$$\delta u_0 : \quad N_{x,x} + N_{xy,y} = I_0 \ddot{u}_0 - I_1 \ddot{w}_{0,x} - J_1 \ddot{\theta}_{,x} \,,$$

$$\delta v_0 : \quad N_{xy,x} + N_{y,y} = I_0 \ddot{v}_0 - I_1 \ddot{w}_{0,y} - J_1 \ddot{\theta}_{,y} \,,$$

$$\delta w_0 : \quad M_{x,xx}^b + 2M_{xy,xy}^b + M_{y,yy}^b$$

$$= I_0 (\ddot{w}_0 + \ddot{\theta}) + I_1 (\ddot{u}_{0,x} \frac{\partial \ddot{u}_0}{\partial x} + \ddot{v}_{0,y}) - I_2 \nabla^2 \ddot{w}_0 - J_2 \ddot{\theta} + J_1^s \ddot{\varphi} \,, \tag{20}$$

$$\delta \theta : \quad - k_1 M_x^s - k_2 M_y^s \; - (k_1 A' + k_2 B') M_{xy,xy}^s + k_1 A' S_{xz,x}^s + k_2 B' S_{yz,y}^s$$

$$= I_0 (\ddot{w}_0 + \ddot{\theta}) + J_1 (\ddot{u}_{0,x} + \ddot{v}_{0,y}) - J_2 \nabla^2 \ddot{w}_0 - K_2 \ddot{\theta} + J_1^s \ddot{\varphi} \,,$$

$$\delta \varphi_z : \quad S_{xz,x}^s + S_{yz,y}^s - N_z = J_1^s (\ddot{w}_0 + \ddot{\theta}) + K_2^s \ddot{\varphi} \,.$$

By putting Eqs. (8) into Eq. (13), and the results obtained into Eq. (17), the resultants of stresses are expressed as:

$$\begin{Bmatrix} N \\ M^b \\ M^s \end{Bmatrix} = \begin{bmatrix} A & B & B^s \\ B & D & D^s \\ B^s & D^s & H^s \end{bmatrix} \begin{Bmatrix} \varepsilon \\ k^b \\ k^s \end{Bmatrix} + \begin{bmatrix} L \\ L^a \\ R \end{bmatrix} \varepsilon_0^z, \quad S = A^s \; \gamma \,,$$

$$N_z = R^a \varphi + L(\varepsilon_x^0 + \varepsilon_y^0) + L^a (k_x^b + k_y^b) + R(k_x^s + k_y^s), \tag{21}$$

where

$$N=\left\{N_x,N_y,N_{xy}\right\},\ M^b=\left\{M_x^b,M_y^b,M_{xy}^b\right\},\ M^s=\left\{M_x^s,M_y^s,M_{xy}^s\right\},$$

$$S=\left\{S_{xz}^s,S_{yz}^s\right\},\ \gamma=\left\{\gamma_{xz},\gamma_{yz}\right\},\ \mathbf{A}^s=\begin{bmatrix}A_{44}^S & 0\\ 0 & A_{55}^S\end{bmatrix},\tag{22}$$

$$\varepsilon=\left\{\varepsilon_x^0,\varepsilon_y^0,\varepsilon_{xy}^0\right\},\qquad k^b=\left\{k_x^b,k_y^b,k_{xy}^b\right\},\qquad k^s=\left\{k_x^s,k_y^s,k_{xy}^s\right\}$$

with

$$A=\begin{bmatrix}A_{11} & A_{12} & 0\\ A_{12} & A_{22} & 0\\ 0 & 0 & A_{66}\end{bmatrix},\quad B=\begin{bmatrix}B_{11} & B_{12} & 0\\ B_{12} & B_{22} & 0\\ 0 & 0 & B_{66}\end{bmatrix},\quad D=\begin{bmatrix}D_{11} & D_{12} & 0\\ D_{12} & D_{22} & 0\\ 0 & 0 & D_{66}\end{bmatrix},$$

$$B^s=\begin{bmatrix}B_{11}^s & B_{12}^s & 0\\ B_{12}^s & B_{22}^s & 0\\ 0 & 0 & B_{66}^s\end{bmatrix},\quad D^s=\begin{bmatrix}D_{11}^s & D_{12}^s & 0\\ D_{12}^s & D_{22}^s & 0\\ 0 & 0 & D_{66}^s\end{bmatrix},\quad H^s=\begin{bmatrix}H_{11}^s & H_{12}^s & 0\\ H_{12}^s & H_{22}^s & 0\\ 0 & 0 & H_{66}^s\end{bmatrix},\tag{23}$$

$$\begin{Bmatrix}L\\ L^a\\ R\\ R^a\end{Bmatrix}=\int_{-h/2}^{h/2}\lambda(z)\begin{Bmatrix}1\\ z\\ f(z)\\ zf(z)\end{Bmatrix}g'(z)dz,$$

$$\begin{Bmatrix}A_{11} & B_{11} & D_{11} & B_{11}^s & D_{11}^s & H_{11}^s\\ A_{12} & B_{12} & D_{12} & B_{12}^s & D_{12}^s & H_{12}^s\\ A_{66} & B_{66} & D_{66} & B_{66}^s & D_{66}^s & H_{66}^s\end{Bmatrix}$$

$$=\int_{-h/2}^{h/2}\lambda(z)\left[1,\ z,\ z^2,f\left(z\right),\ zf\left(z\right),f^2\left(z\right)\right]\begin{Bmatrix}\dfrac{1-\nu}{\nu}\\ 1\\ \dfrac{1-2\nu}{2\nu}\end{Bmatrix}\ dz,\tag{24a}$$

$$A_{44}^s=A_{55}^s=\int_{-h/2}^{h/2}\mu(z)\ [g(z)]^2\ dz,\tag{24b}$$

$$(A_{22},\ B_{22},\ D_{22},\ B_{22}^s,\ D_{22}^s,\ H_{22}^s)=(A_{11},\ B_{11},\ D_{11},\ B_{11}^s,\ D_{11}^s,\ H_{11}^s).\tag{24c}$$

By putting Eqs. (9) and (10) into Eq. (21), and the results obtained into Eq. (20), the motion equations can be determined in terms of displacements ($\delta u_0,\delta v_0,\delta w_0,\delta\theta,\delta\varphi_z$) as

$$A_{11}u_{0,xx}+A_{12}v_{0,xy}+A_{66}\left(u_{0,yy}+v_{0,xy}\right)-B_{11}w_{0,xxx}-B_{12}w_{0,xyy}\ -2B_{66}w_{0,xyy}$$

$$+B_{11}^sA'k_1\theta_{,xxx}B_{12}^sB'k_2\theta_{,xyy}+B_{66}^s\left(A'k_1+B'k_2\right)\theta_{,xyy}+L\varphi_{z,x}=I_0\ddot{u}_0-I_1\ddot{w}_{0,x}-J_1\ddot{\theta}_{,x},\tag{25a}$$

$$A_{12}u_{0,xy}+A_{22}v_{0,yy}+A_{66}\left(u_{0,xy}+v_{0,xx}\right)-B_{12}w_{0,xxy}-B_{22}w_{0,yyy}\ -2B_{66}w_{0,xxy}$$

$$+B_{12}^sA'k_1\theta_{,xxy}+B_{22}^sB'k_2\theta_{,yyy}+B_{66}^s\left(A'k_1+B'k_2\right)\theta_{,xxy}+L\varphi_{z,y}$$

$$=I_0\ddot{v}_0-I_1\ddot{w}_{0,y}-J_1\ddot{\theta}_{,y},\tag{25b}$$

$$B_{11}u_{0,xxx}+B_{12}\left(u_{0,xyy}+v_{0,xxy}\right)+B_{22}v_{0,yyy}+2B_{66}\left(u_{0,xyy}+v_{0,xxy}\right)-D_{11}w_{0,xxxx}$$
$$-2D_{12}w_{0,xxyy}-D_{22}w_{0,yyyy}-4D_{66}w_{0,xxyy}+D_{11}^{s}A'k_1\theta_{,xxxx}+D_{12}^{s}\left(A'k_1+B'k_2\right)\theta_{,xxyy}$$
$$+D_{22}^{s}B'k_2\theta_{,yyyy}+2D_{66}^{s}\left(A'k_1+B'k_2\right)\theta_{,xxyy}+L^{a}(\varphi_{z,xx}+\varphi_{z,yy})$$
$$=I_0(\ddot{w}_0+\ddot{\theta})+J_1(\ddot{u}_{0,x}+\ddot{v}_{0,y})-J_2\ddot{w}_{0,xxyy}-K_2\ddot{\theta}_{,xxyy}+J_1^{s}\ddot{\varphi}, \tag{25c}$$

$$-B_{11}^{s}A'k_1u_{0,xxx}-B_{12}^{s}\left(A'k_1v_{0,xxy}+B'k_2u_{0,xyy}\right)-B_{22}^{s}B'k_2v_{0,yyy}$$
$$-B_{66}^{s}\left(\left(A'k_1+B'k_2\right)u_{0,xyy}+\left(A'k_1+B'k_2\right)v_{0,xxy}\right)+D_{11}^{s}A'k_1w_{0,xxxx}$$
$$+D_{12}^{s}\left(A'k_1+B'k_2\right)w_{0,xxyy}+D_{22}^{s}B'k_2w_{0,yyyy}+2D_{66}^{s}\left(A'k_1+B'k_2\right)w_{0,xxyy}$$
$$-H_{11}^{s}\left(A'k_1\right)^2\theta_{,xxxx}-2H_{12}^{s}A'k_1B'k_2\theta_{,xxyy}-H_{22}^{s}\left(B'k_2\right)^2\theta_{,yyyy}$$
$$-H_{66}^{s}\left(A'k_1+B'k_2\right)^2\theta_{,xxyy}+A_{44}^{s}\left(A'k_1\right)^2\theta_{,xx}+A_{55}^{s}\left(B'k_2\right)^2\theta_{,yy}+R(\varphi_{z,xx}+\varphi_{z,yy})$$
$$+A_{44}^{s}\varphi_{z,xx}+A_{55}^{s}\varphi_{z,yy}=I_0(\ddot{w}_0+\ddot{\theta})+J_1(\ddot{u}_{0,x}+\ddot{v}_{0,y})-J_2\ddot{w}_{0,xxyy}-K_2\ddot{\theta}_{,xxyy}+J_1^{s}\ddot{\varphi}, \tag{25d}$$
$$L(u_{0,x}+v_{0,y})-L^{a}(w_{0,xx}+w_{0,yy})-(R+A_{44}^{s})\theta_{,xx}-(R+A_{55}^{s})\theta_{,yy}$$
$$+R^{a}\varphi-A_{44}^{s}\varphi_{z,xx}-A_{55}^{s}\varphi_{z,yy}=J_1^{s}(\ddot{w}_0+\ddot{\theta})+K_2^{s}\ddot{\varphi}. \tag{25e}$$

2.5. Exact solution for simply supported FG plate

Generally, the rectangular plates can be classified based on the type of support used. In this study, the exact solutions of Eqs. (25a)-(25e) for a simply supported FG plate is considered.

The boundary conditions at the edges of the plate are expressed as follows:

$$\begin{aligned} &v_0=w_0=\theta=\theta_{,y}=\varphi=N_x=M_x^{b}=M_x^{s}=0 \text{ at } x=0,\ a,\\ &u_0=w_0=\theta=\theta_{,x}=\varphi=N_y=M_y^{b}=M_y^{s}=0 \text{ at } y=0,\ b. \end{aligned} \tag{26}$$

The procedure of the Navier's solution in this study is obtained by assuming the following solution $\left(\delta u_0,\delta v_0,\delta w_0,\delta\theta,\delta\varphi_z\right)$ that satisfies the boundary conditions in Eq. (26):

$$\begin{Bmatrix} u_0\\ v_0\\ w_0\\ \theta\\ \varphi^{z} \end{Bmatrix}=\sum_{m=1}^{\infty}\sum_{n=1}^{\infty}\begin{Bmatrix} U_{mn}e^{iwt}\cos(\alpha\ x)\sin(\beta\ y)\\ V_{mn}e^{iwt}\sin(\alpha\ x)\cos(\beta\ y)\\ W_{mn}e^{iwt}\sin(\alpha\ x)\sin(\beta\ y)\\ X_{mn}e^{iwt}\sin(\alpha\ x)\sin(\beta\ y)\\ \Phi_{mn}e^{iwt}\sin(\alpha\ x)\sin(\beta\ y) \end{Bmatrix}, \tag{27}$$

where U_{mn}, V_{mn}, W_{mn}, X_{mn}, and Φ_{mn} are the arbitrary parameters to be determined, ω is the natural frequency, α, β are defined as:

$$\alpha=m\pi/a \text{ and } \beta=n\pi/b. \tag{28}$$

By putting Eqs. (27) and (28) into Eq. (25), the analytical solutions can be determined from

$$\left(\begin{bmatrix} a_{11} & a_{12} & a_{13} & a_{14} & a_{15} \\ a_{12} & a_{22} & a_{23} & a_{24} & a_{25} \\ a_{13} & a_{23} & a_{33} & a_{34} & a_{35} \\ a_{14} & a_{24} & a_{34} & a_{44} & a_{45} \\ a_{15} & a_{25} & a_{35} & a_{45} & a_{55} \end{bmatrix} - \omega^2 \begin{bmatrix} m_{11} & 0 & m_{13} & m_{14} & 0 \\ 0 & m_{22} & m_{23} & m_{24} & 0 \\ m_{13} & m_{23} & m_{33} & m_{34} & m_{35} \\ m_{14} & m_{24} & m_{34} & m_{44} & m_{45} \\ 0 & 0 & m_{35} & m_{45} & m_{55} \end{bmatrix}\right) \begin{Bmatrix} U_{mn} \\ V_{mn} \\ W_{mn} \\ X_{mn} \\ \Phi_{mn} \end{Bmatrix} = \begin{Bmatrix} 0 \\ 0 \\ 0 \\ 0 \\ 0 \end{Bmatrix}, \tag{29}$$

in which

$$\begin{gathered} a_{11} = -(A_{11}\alpha^2 + A_{66}\beta^2),\ a_{22} = -\alpha^2 A_{66} - \beta^2 A_{22}, \\ a_{33} = -\alpha^2\left(D_{11}\alpha^2 + \left(2D_{12} + 4D_{66}\right)\beta^2\right) - D_{22}\beta^4, \\ a_{44} = -(H_{11}^s\alpha^2 k_1 + 2k_1\beta^2 H_{66}^s + 2H_{66}^s\alpha^2 k_2 + H_{12}^s\alpha^2 k_2 \\ +k_1\beta^2 H_{12}^s + k_2\beta^2 H_{22}^s + A_s^{44}k_1 + A_s^{55}k_2), \\ a_{55} = -(A_{44}^s\alpha^2 + A_{55}^s\beta^2 + R^a), \\ a_{12} = -\alpha\ \beta\ \left(A_{12} + A_{66}\right), \\ a_{13} = \alpha(B_{11}\alpha^2 + (B_{12} + 2B_{66})\beta^2), \\ a_{14} = -\alpha(B_{11}^s A'k_1\alpha^2 + B_{12}^s B'k_2\beta^2 + B_{66}^s\left(A'k_1 + B'k_2\right)\beta^2), \\ a_{15} = L\alpha,\ a_{25} = L\beta,\ a_{35} = -L^a(\alpha^2 + \beta^2),\ a_{45} = -[A_{44}^s\alpha^2 + A_{55}^s\beta^2 + R(\alpha^2 + \beta^2)], \\ a_{22} = -\alpha^2 A_{66} - \beta^2 A_{22}, \\ a_{23} = \beta(B_{22}\beta^2 + (B_{12} + 2B_{66})\alpha^2), \\ a_{24} = -\beta\left\{B_{22}^s B'k_2\beta^2 + \alpha^2\left[B_{12}^s A'k_1 + B_{66}^s\left(A'k_1 + B'k_2\right)\right]\right\}, \\ a_{34} = D_{11}^s A'k_1\alpha^4 + D_{12}^s\left(A'k_1 + B'k_2\right)\beta^2\alpha^2 + D_{22}^s B'k_2\beta^4 + 2D_{66}^s\left(A'k_1 + B'k_2\right)\beta^2\alpha^2, \end{gathered} \tag{30}$$

and

$$\begin{gathered} m_{11} = m_{22} = -I_0,\ m_{33} = -[I_0 + I_2(\alpha^2 + \beta^2)], \\ m_{44} = -[I_0 + K_2(\alpha^2 + \beta^2)],\ m_{55} = -K_2^s, \\ m_{13} = \alpha I_1, m_{14} = \alpha J_1, \\ m_{23} = \beta I_1,\ m_{24} = \beta J_1, \\ m_{34} = -[I_0 + J_2(\alpha^2 + \beta^2)], \qquad m_{35} = m_{45} = -J_1^s. \end{gathered} \tag{31}$$

3. Numerical Results

This Section presents several numerical examples for the free vibration analyses of a simply supported FG plate. Firstly, the model proposed will be validated by means of comparison with the data available in the literature. For this,

TABLE 1. Material Proprieties Used in the FG Plates

Proprieties	Metal		Ceramic	
	Al	Al*	Al_2O_3	ZrO_2*
E, GPa	70	68.9	380	211
v	0.3	0.3	0.3	0.3
P, kg/m^3	2702	2700	3800	4500

TABLE 2. Comparison of Normalized Natural Frequencies $\bar{\omega}$ for Isotropic Square Plate ($a/h = 10$).

Method	ε_z	Mode (m, n)							
		(1, 1)	(1, 2)	(2, 2)	(1, 3)	(2, 3)	(3, 3)	(2, 4)	(1, 5)
[41]	$\neq 0$	0.0932	0.2226	0.3421	0.4172	0.5240	0.6892	0.7515	0.9275
[42]	$\neq 0$	0.0933	0.2228	0.3422	0.4173	0.5240	0.6890	0.7512	0.9268
[49]	$\neq 0$	0.0932	0.2226	0.3421	0.4171	0.5239	0.6889	0.7511	0.9268
[50]	$= 0$	0.0930	0.2220	0.3406	0.4149	0.5206	0.6834	0.7447	0.9174
Present 2D	$= 0$	0.0930	0.2219	0.3406	0.4151	0.5208	0.6840	0.7454	0.9187
Present 3D	$\neq 0$	0.0931	0.2226	0.3421	0.4172	0.5240	0.6892	0.7515	0.9275

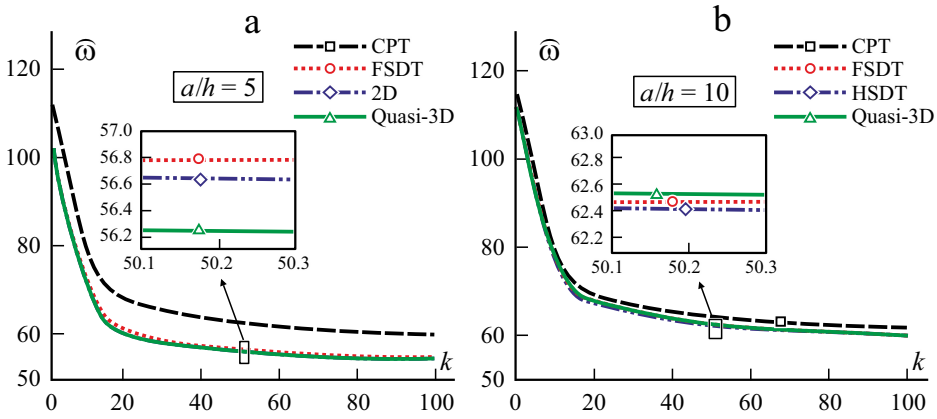

Fig. 2. Variation of the first dimensionless frequency $\bar{\omega}$ as a function of material index k of square FG plate with side-to-thickness ratio a/h = 5 (a) and 10 (b).

two types of FGMs plates are assumed: Al/Al_2O_3 and (Al)*/ (ZrO_2)*. Table 1 presents the properties of the FG plates. For convenience, the current normalized natural frequency forms are used:

$$\bar{\omega} = \omega\pi^2\left(a^2/h\right)\sqrt{\rho_m/E_m}\ ,\ \bar{\omega} = \omega a^2/2\pi\sqrt{\rho h/D}\ ,\ \tilde{\omega} = \omega h\sqrt{\rho_c/E_c}\ ,$$

$$\breve{\omega} = \omega h\sqrt{\frac{\rho}{G}}\ ,\ \bar{\Omega} = \Omega\left(\frac{b^2}{h}\right)\sqrt{\rho_0/E_0}\ ,\ \tilde{\Omega} = \Omega\left(\frac{a^2}{h}\right)\sqrt{\rho_c/E_c}\ . \tag{32}$$

To study the effectiveness of the present theories, many comparative studies are presented in the next Section. In Table 2, the normalized natural frequencies calculated and the results obtained by the quasi-3D models of Jha et al. [41] and Hebali et al. [42], the exact 3D solution of Srinivas et al. [48], and FSDT of Whitney and Pagano [49] are compared. The results demonstrate that the current theories (2D and quasi-3D) agree with those determined by the other theories for all vibration modes.

TABLE 3. Normalized Natural Frequencies $\widehat{\omega}$ of Thin Plate with Various Gradient Indices ($h/\mathrm{a} = 0.01$, $a/b = 1$)

Gradient index	Method	Mode (m, n)				
		1	2	3	4	5
$k = 0$	CPT [51]	115.9252	289.7795	289.7795	463.5892	579.468
	FSDT [51]	115.8926	289.5809	289.5809	463.0745	578.7338
	Present 2D	115.7854	289.3056	289.3056	462.6369	578.0866
	Present 3D	115.7870	289.3158	289.3158	462.6630	578.1271
$k = 0.5$	CPT [51]	101.7838	254.4306	254.4306	407.0386	508.7825
	FSDT [51]	98.13488	245.2213	245.2213	392.1553	490.1263
	Present 2D	98.0682	245.0491	245.0491	391.8845	489.6943
	Present 3D	98.7054	246.6456	246.6456	394.4443	492.8985
$k = 1$	CPT [51]	96.40367	240.9814	240.9814	385.522	481.8871
	FSDT [51]	88.42912	220.9715	220.9715	353.3795	441.6718
	Present 2D	88.3813	220.8452	220.8452	353.1801	441.3316
	Present 3D	89.6946	224.1296	224.1296	358.4368	447.9040
$k = 2$	CPT [51]	92.1328	230.3048	230.3048	368.4405	460.535
	FSDT [51]	80.39669	200.8961	200.8961	321.2691	401.533
	Present 2D	80.3647	200.8060	200.8060	321.1202	401.2595
	Present 3D	82.1826	205.3494	205.3494	328.3878	410.3423

TABLE 4. Normalized Natural Frequencies $\widehat{\omega}$ of Thin Plate with Various Gradient Indices ($h/\mathrm{a} = 0.01$, $a/b = 2$)

Gradient index	Method	Mode (m, n)				
		1	2	3	4	5
$k = 0$	CPT [51]	72.45548	115.9255	188.375	246.321	289.7797
	FSDT [51]	72.44281	115.8973	188.3682	246.1798	289.5828
	Present 2D	72.3264	115.6593	187.7762	245.3760	288.5213
	Present 3D	72.3290	115.6658	187.7932	245.4051	288.5618
$k = 0.5$	CPT [51]	63.61681	101.7841	165.3958	216.2733	254.4307
	FSDT [51]	61.34204	98.13939	159.5172	208.4666	245.2231
	Present 2D	61.2623	97.9712	159.0721	207.8808	244.4452
	Present 3D	61.6614	98.6111	160.1158	209.2493	246.0585
$k = 1$	CPT [51]	60.25416	96.40398	156.6532	204.8412	240.9816
	FSDT [51]	55.27501	88.43342	143.7455	187.851	220.9732
	Present 2D	55.2113	88.2950	143.3630	187.3533	220.3086
	Present 3D	56.0324	89.6092	145.4997	190.1485	223.5982
$k = 2$	CPT [51]	57.58483	92.13309	149.7129	195.7659	230.3049
	FSDT [51]	50.25433	80.40054	130.6866	170.7853	200.8976
	Present 2D	50.2015	80.2801	130.3409	170.3266	200.2793
	Present 3D	51.3374	82.0970	133.2920	174.1843	204.8167

The first five modes of the normalized natural frequencies for two values of aspect ratio ($a/b = 1$, $a/b = 2$), respectively, are presented in Tables 3 and 4. The results given by Yin et al. [37] and the results obtained by the current approaches (2D and quasi-3D) are compared. The fundamental frequencies calculated by the present methods match better than those from Yin et al. [37] based on the CPT and FSDT.

TABLE 5. Comparisons of Fundamental Frequency Parameters $\bar{\omega}$ of Simply Supported Isotropic Rectangular Plates with Other Theories ($b = 2a$).

Method	h/b				
	0.005	0.01	0.02	0.1	0.2
CPT [52]	1.96339	1.9631	1.96188	1.92433	1.81954
FSDT [52]	1.96305	1.9617	1.95639	1.80958	1.51101
Present 2D	1.9630	1.9617	1.9564	1.8099	1.5195
Present 3D	1.9631	1.9618	1.9567	1.8152	1.5320

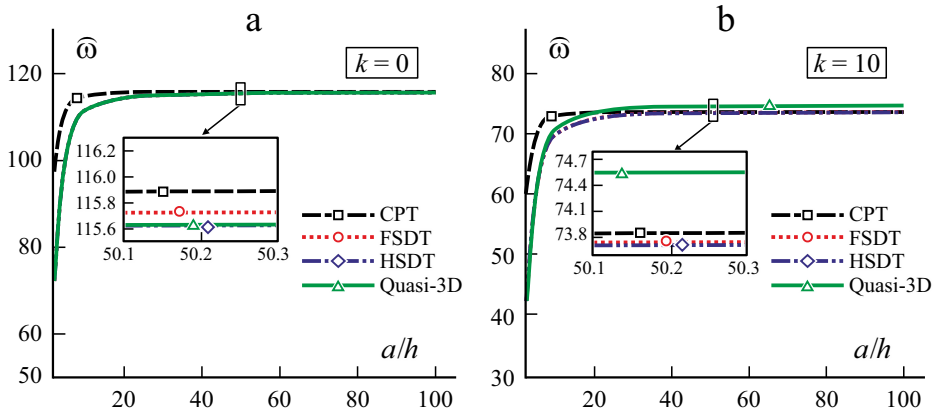

Fig. 3. Variation of dimensionless fundamental frequency $\bar{\omega}$ vs. aspect ratio a/h for the index material k = 0 (a) and 10 (b) (at a/b =1).

For thick plates, the CPT and FSDT theories cannot provide the results as accurately as 2D and quasi-3D approaches, because the 2D and quasi-3D do not depend on any hypothesis compared with CPT and FSDT theories, see Table 5. The present theories generally give a good estimation for normalized natural frequencies in thick FG plates, where the impacts of stretching and shear strain are important.

Figure 2 compares the fundamental frequency of the square FG plates calculated by different theories. The solutions based on the CPT and other theories are close to each other for high values of side-to-thickness ratio a/h. A significant difference exists between the CPT and the other theories for small values of side-to-thickness ratio a/h. However, the divergence in the quasi-3D case is faster than the 2D and FSDT theories because of the effect stretching. The side-to-thickness ratio has an insignificant impact on the change between the CPT and the other shear deformation theories.

Figure 3 presents the variation of the fundamental frequency of the square plate for three values of gradient index k in terms of side-to-thickness a/h and various theories (CPT, FSDT, HSDT, and Quasi-3D). The solutions obtained by the CPT and HSDT are near each other for small or large gradient indices. The material appears relatively homogeneous for small or large gradient indexes. However, the material is nonhomogeneous for moderate gradient indexes. In addition, this difference is due to the effects of transverse shear strains taken into account in the cases of HSDT, and it appears in the Quasi-3D theory due to the stretching effect.

Figure 4 illustrates the variation of the fundamental frequency of the square plate for three values of gradient index k in terms of side-to-thickness b/h and for different theories (CPT, FSDT, HSDT, and Quasi-3D). For the three cases, the fundamental frequencies decrease with the increasing the side-to-thickness ratio. Consequently, the difference between the CPT and the other theories increases because of the effect of shear strains. The small difference between Quasi-3D, FSDT, and HSDT is due to the stretching effect.

Figure 5 demonstrates the fundamental frequency variation of simply supported FG plate versus the aspect ratio b/a for different values of the side-to-thickness ratios a/h. The highest frequencies are obtained for a square plate (b/a = 1).

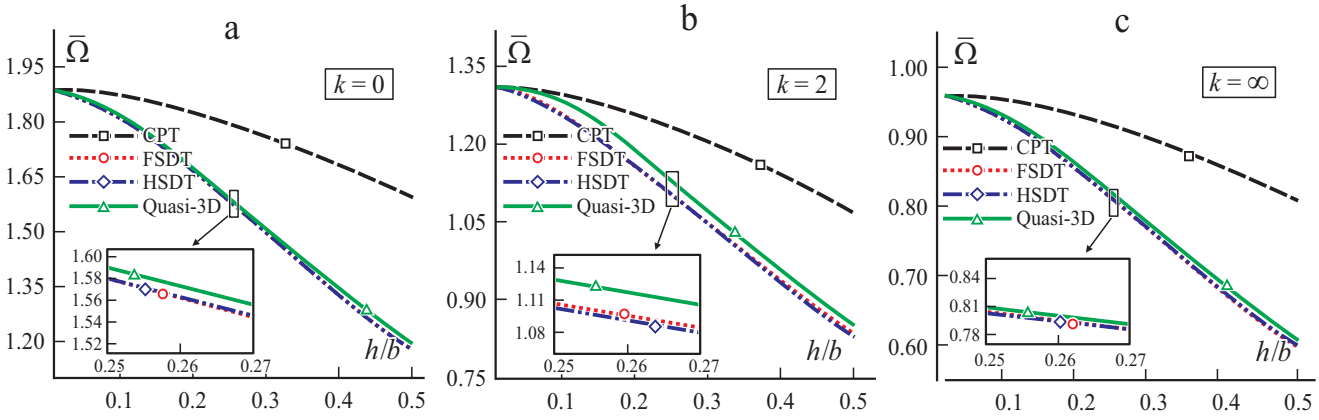

Fig. 4. Variation of dimensionless fundamental frequency $\bar{\Omega}$ vs. the side-to-thickness ratio h/b for various values of index material k = 0 (a), 2 (b), and ∞ (c); (at a/b =1).

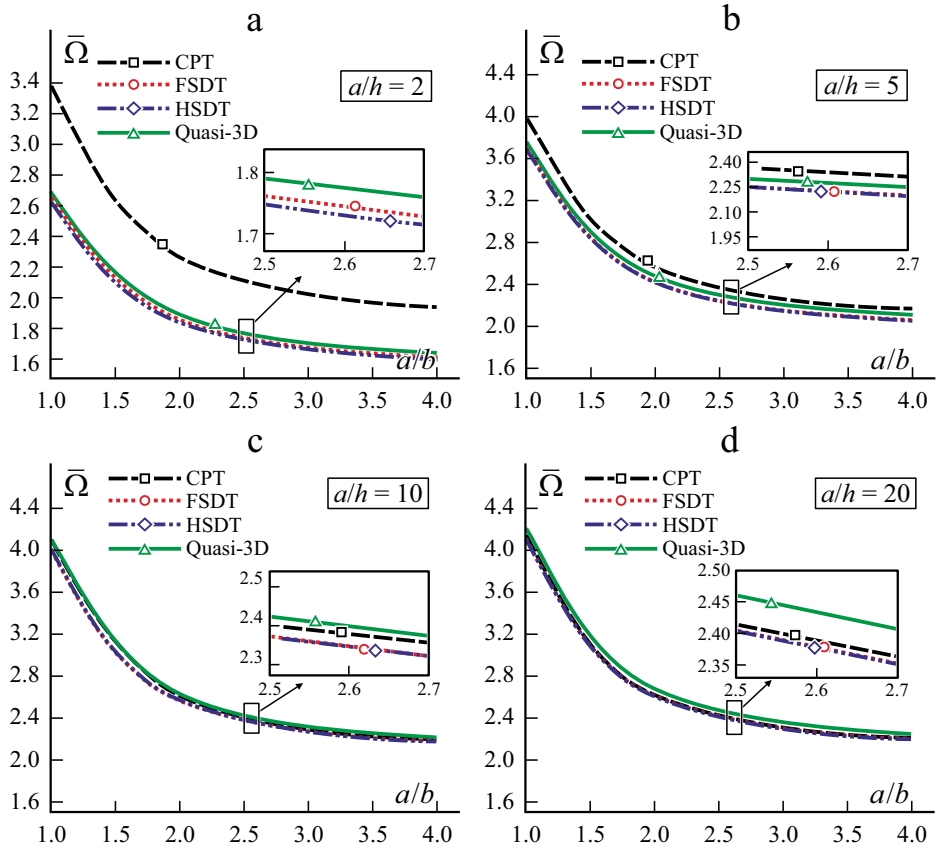

Fig. 5. Variation of dimensionless fundamental frequency parameter $\bar{\Omega}$ vs. the aspect ratios a/b for various values of side-to-thickness ratio a/h = 2 (a), 5 (b), 10 (c), and 20 (d); (at k = 2).

They decrease with the increasing the aspect ratio b/a for all theories. The results obtained using the different theories get closer with the rise in the side-to-thickness ratio a/h and have almost the same values, except for the Quasi-3D theory.

Figure 6 illustrates the fundamental frequencies of various plates versus the geometrical ratio a/b using different shear theories. The highest frequencies are obtained for a ceramic square plate (a/b = 1). Whatever the shear theory class,

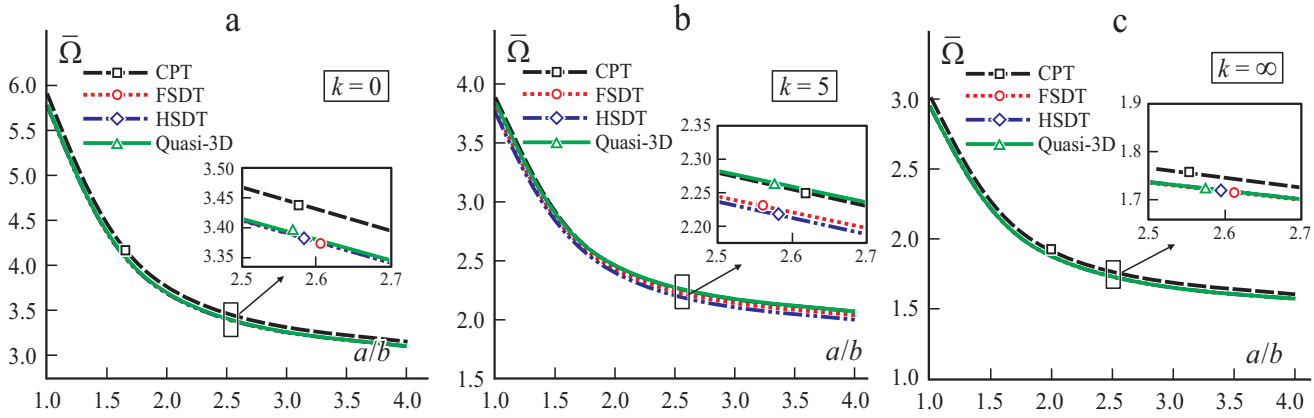

Fig. 6. Variation of dimensionless fundamental frequency $\bar{\Omega}$ vs. the ratio a/b for various values of material index k = 0 (a), 5 (b), and ∞; (at a/h = 10).

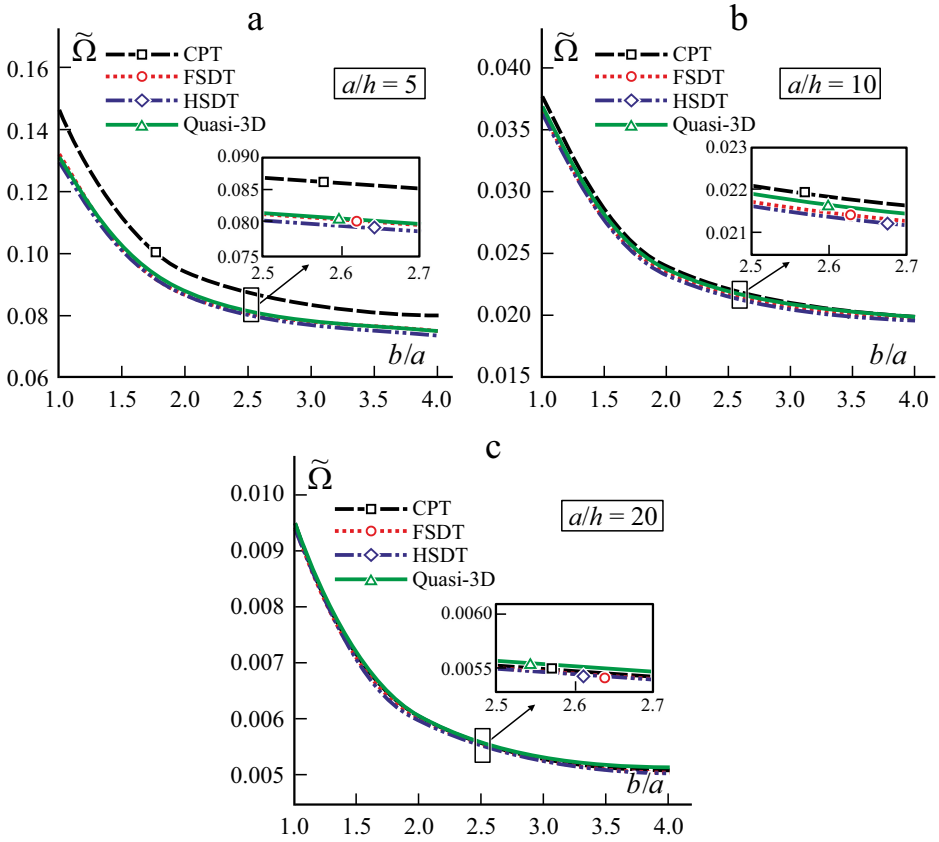

Fig. 7. Variation of dimensionless fundamental frequency parameter $\tilde{\Omega}$ vs. the ratio b/a for various values side to thickness ratio a/h = 5 (a), 10 (b), and 20 (c); (at k = 10).

all the curves exhibit almost the same evolution. The fundamental frequencies fall rapidly when the geometrical ratio is small ($a/b < 2.5$), while they slowly decrease when $a/b > 2.5$.

Figure 7 presents the variation of the fundamental frequency of the FG plate as a function of aspect ratio b/a for different values of side to thickness a/h. The maximum frequencies are obtained for a square plate (b/a = 1) and decrease

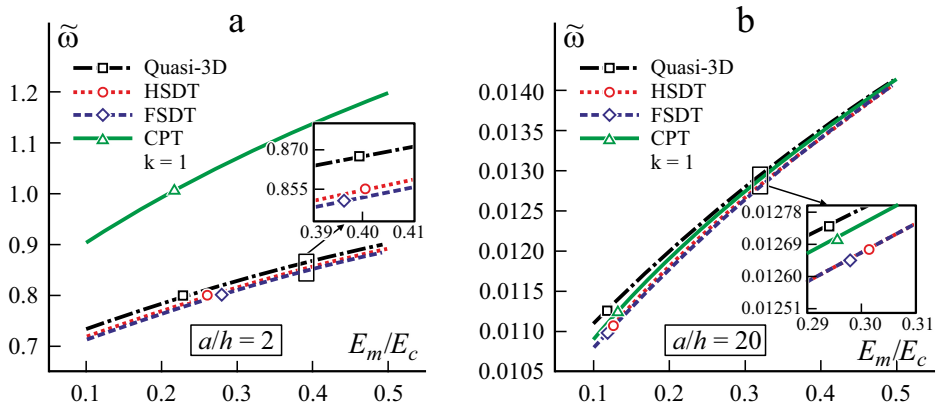

Fig. 8. Variation of dimensionless fundamental frequency $\tilde{\omega}$ of simply supported FG plates vs. anisotropy ratio E_m/E_c for $a/h = 2$ (a) and 20 (b); (at $k = 1$, $b/a = 1$).

with the aspect ratio b/a increasing for all theories. The results obtained using the different theories get closer with the rise in the side-to-thickness ratio a/h and have almost the same values, except for the Quasi-3D theory, which comes down to the stretching effect.

Figure 8 illustrates the influence of the various theories on dimensionless natural frequency. The normalized fundamental frequency values converge towards the same value for a thinner plate regardless of the theory employed. The slight difference between HSDT and FSDT is due to the estimation of shear stresses and stretching effect.

4. Conclusion

Quasi-3D and 2D free vibration analyses were performed using linear small strain elasticity theory. The current mathematical method can ensure the accurate solutions for thick plates, better approximating the previous approximate plate theories (CPT and FSDT). In addition, the power-law FGM plates are employed. The accuracy of the method presented is also validated by comparing the results of this study with other theories. Briefly, the following conclusions can be formulated.

There is good agreement between the results obtained by the models presented and the available in literature. Furthermore, the fundamental frequency decreases with increasing the material index; simultaneously, the difference between the models disappears with increasing the side-to-thickness ratio.

For high values of side-to-thickness, the quasi-3D theory of inhomogeneous plate presents a significant difference compared with other models due to the stretching effect. However, for the homogeneous thin plates, the values of the frequencies converge towards the same values.

The fundamental frequencies increase with decreasing the side-to-thickness ratio and increasing the aspect ratio.

Increasing the anisotropy ratio increases the normalized natural frequency, and the transverse shear strains can be neglected in thin plates.

A parametric study for plate side-to-thickness ratios, aspect ratios, and material index indicates that thin plates are slightly more sensitive to material properties than thick plates. Therefore, both models utilized in the present work ensure a good prediction for normalized natural frequencies, whatever the plate thickness.

Finally, it is concluded that the specific dimensional effect of quasi-3D HSDT theory, through-thickness stretching, significantly affects the free vibrations of the FG advanced composite plates. Therefore, the resulting negative impacts of stretching thickness are reduced by adopting suitable quasi-3D theories.

REFERENCES

1. Y. Uchida, "Properties of functionally graded materials, Manufactured by progressive lamination method for applications", Aichi Inst, Technol. Res. Rep (2004), 39-51.
2. L. Marin, "Numerical solution of the Cauchy problem for steady-state heat transfer in two-dimensional functionally graded materials". Int. J. Solids and Struct.," **42**, No. 15, 4338-4351 (2005).
3. Z. Liu, M. A. Meyers, Z. Zhang, and R. O. Ritchie, "Functional gradients and heterogeneities in biological materials: Design principles, functions, and bioinspired applications," Progress in Mater. Sci., **88**, 467-498 (2017).
4. L. Bai, C. Gong, X. Chen, Y. Sun, J. Zhang, L. Cai, and S. Q. Xie, "Additive manufacturing of customized metallic orthopedic implants: Materials, structures, and surface modifications," Metals, **9**, No. 9, 1004 (2019).
5. S. H. Chi and T. L. Chung, "Cracking in coating–substrate composites with multi-layered and FGM coatings," Eng. Fracture Mech., **70**, No. 10, 1227-1243 (2003).
6. H. Shi, P. Zhou, J. Li, C. Liu and L. Wang, "Functional gradient metallic biomaterials: Techniques, current scenery, and future prospects in the biomedical field," Frontiers in Bioeng. and Biotechnol., **8**, 616845 (2021).
7. F. Y. Genao, J. Kim, and K. K. Żur, "Nonlinear finite element analysis of temperature-dependent functionally graded porous micro-plates under thermal and mechanical loads," Compos. Struct., **256**, 112931 (2021).
8. N. V. Nguyen, H. Nguyen-Xuan, D. Lee, and J. Lee, "A novel computational approach to functionally graded porous plates with graphene platelets reinforcement," Thin-Walled Struct., **150**, 106684 (2020).
9. K. Xie, Y. Wang, H. Niu, and H. Chen, "Large-amplitude nonlinear free vibrations of functionally graded plates with porous imperfection: A novel approach based on energy balance method," Compos. Struct., **246**, 112367 (2020).
10. Y. Zhang, G. Jin, M. Chen, T. Ye, C. Yang, and Y. Yin, "Free vibration and damping analysis of porous functionally graded sandwich plates with a viscoelastic core," Compos. Struct., **244**, 112298 (2020).
11. Y. S. Al Rjoub and A. A. Jinan, "Free vibration of functionally-graded porous cracked plates," Structures, **28**, 2392-2403 (2020).
12. A. Bouhadra, A. Tounsi, A. A. Bousahla, S. Benyoucef, and S. R. Mahmoud, "Improved HSDT accounting for effect of thickness stretching in advanced composite plates," Int. J. Struct. Eng. and Mech., **66**, No. 1, 61-73 (2018).
13. B. Rebai, A. Bouhadra, A. A. Bousahla, M. Meradjah, F. Bourada A. Tounsi, and M. Hussain, "Thermoelastic response of functionally graded sandwich plates using a simple integral HSDT," Archive of Appl. Mech., **91**, No. 7, 3403-3420 (2021).
14. N. V. Nguyen, L. B. Nguyen, H. Nguyen-Xuan and J. Lee, "Analysis and active control of geometrically nonlinear responses of smart FG porous plates with graphene nanoplatelets reinforcement based on Bézier extraction of NURBS," Int. J. Mech. Sci., **180**, 105692 (2020).
15. A. Bouhadra, A. Menasria, and M. A. Rachedi, "Boundary conditions effect for buckling analysis of porous functionally graded nanobeam," Adv. Nano Research, **10**, No. 4, 313-325 (2021).
16. E. Arshid and A. R. Khorshidvand, "Free vibration analysis of saturated porous FG circular plates integrated with piezoelectric actuators via differential quadrature method," Thin-Walled Struct., **125**, 220-233 (2018).
17. N. Valizadeh, T. Q. Bui, V. T. Vu, H. T. Thai, and M. N. Nguyen, "Isogeometric simulation for buckling, free and forced vibration of orthotropic plates," Int. J. Appl. Mech., **5**, No. 02, 1350017 (2013).
18. Z. Hashin, "Analysis of composite materials—a survey," J. Appl. Mech., **50**, 481-505 (1983).
19. J. N. Reddy and J. Berry, "Nonlinear theories of axisymmetric bending of functionally graded circular plates with modified couple stress," Compos. Struct., **94**, No. 12, 3664-3668 (2012).
20. E. Reissner and Y. Stavsky, "Bending and stretching of certain types of heterogeneous aeolotropic elastic plates," J. Appl. Mech., **28**. No. 3, 402-408 (1961).
21. M. Mohammadi, A. R. Saidi, and E. Jomehzadeh, "Levy solution for buckling analysis of functionally graded rectangular plates," Appl. Compos. Mater., **17**, No. 2, 81-93 (2010).
22. S. Zghal, A. Frikha, and F. Dammak, "Large deflection response-based geometrical nonlinearity of nanocomposite structures reinforced with carbon nanotubes," Appl. Math. and Mech., **41**, No. 8, 1227-1250 (2020).
23. K. Mercan, A. K. Baltacioglu, and Ö. Civalek, "Free vibration of laminated and FGM/CNT composites annular thick plates with shear deformation by discrete singular convolution method," Compos. Struct., **186**, 153 (2018).

24. H. Mellouli, H. Jrad, M. Wali, and F. Dammak, "Meshless implementation of arbitrary 3D-shell structures based on a modified first order shear deformation theory," Computers & Math. with Applications, **77**, No. 1, 34-49 (2019).
25. S. Trabelsi, A. Frikha, S. Zghal, and F. Dammak, "Thermal post-buckling analysis of functionally graded material structures using a modified FSDT," Int. J. Mech. Sci., **144**, 74-89 (2018).
26. F. Ebrahimi and N. Shafiei, "Application of Eringen's nonlocal elasticity theory for vibration analysis of rotating functionally graded nanobeams," Smart Struct. and Systems, **17**, No. 5, 837-857 (2016).
27. Y. Zhou and J. Zhu, "Vibration and bending analysis of multiferroic rectangular plates using third-order shear deformation theory," Compos. Struct., **153**, 712-723 (2016).
28. O. Bourihane, Y. Hilali, and K. Mhada, "Nonlinear dynamic response of functionally graded material plates using a high-order implicit algorithm," ZAMM-J. Appl. Math. and Mech./Zeitschrift für Angewandte Mathematik und Mechanik, **100**, No. 12, e202000087 (2020).
29. Y. Zhou, D. Liu, and J. Zhu, "Vibration and wave analyses in the functionally graded graphene-reinforced composite plates based on the first-order shear deformation plate theory," Appl. Sci., **12**, No. 6, 3140 (2022).
30. R. Kang, F. Xin, C. Shen, and T. J. Lu, "3D free vibration analysis of functionally graded plates with arbitrary boundary conditions in thermal environment," Adv. Eng. Mater., **24**, No. 5, 2100636 (2022).
31. Y. XU and Z. WU, "Exact solutions for rectangular anisotropic plates with four clamped edges," Mech. Adv. Mater. and Struct., **29**, No. 12, 1756-1768 (2022).
32. T. V. Vu, A. Khosravifard, M. R. Hematiyan, and T. Q. Bui, "A new refined simple TSDT-based effective meshfree method for analysis of through-thickness FG plates," Appl. Math. Model., **57**, 514-534 (2018).
33. D. Shahsavari, M. Shahsavari, L. Li, and B. Karami, "A novel quasi-3D hyperbolic theory for free vibration of FG plates with porosities resting on Winkler/Pasternak/Kerr foundation," Aerospace Sci. and Technol., **72**, 134-149 (2018).
34. M. Arefi, A. Tabatabaeian, and M. Mohammadi, "Bending and stress analysis of polymeric composite plates reinforced with functionally graded graphene platelets based on sinusoidal shear-deformation plate theory," Defence Technol., **17**, No. 1, 64-74 2021.
35. Y. WANG and D. WU, "Free vibration of the functionally graded porous cylindrical shell using a sinusoidal shear deformation theory," Aerospace Sci. and Technol., **66**, 83-91 (2017).
36. S. Alimirzaei, M. Sadighi, and A. Nikbakht, "Wave propagation analysis in viscoelastic thick composite plates resting on visco-Pasternak foundation by means of quasi-3D sinusoidal shear deformation theory," Eur. J. Mech.-A/Solids, **74**, 1-15 (2019).
37. J. Si and Y. Zhang, "An enhanced higher order zigzag theory for laminated composite plates under mechanical/thermal loading," Compos. Struct., **282**, 115074 (2022).
38. M. Sorrenti and M. Di Sciuva, "An enhancement of the warping shear functions of Refined Zigzag Theory," J. Appl. Mech., **88**, No. 8, (2021).
39. A. Tessler, "Refined zigzag theory for homogeneous, laminated composite, and sandwich beams derived from Reissner's mixed variational principle," Meccanica, **50**, No. 10, 2621-2648 (2015).
40. P. Jafari and Y. Kiani, "Free vibration of functionally graded graphene platelet reinforced plates: A quasi 3D shear and normal deformable plate model," Compos. Struct., **275**, 114409 (2021).
41. D. K. Jha, T. Kant, and R. K. Singh, "Free vibration response of functionally graded thick plates with shear and normal deformations effects," Compos. Struct., **96**, 799-823 (2013).
42. H. Hebali, A. Tounsi, M. S. A. Houari, A. Bessaim, and E. A. A. Bedia, "New quasi-3D hyperbolic shear deformation theory for the static and free vibration analysis of functionally graded plates," J. Eng. Mech., **140**, No 2, 374-383 (2014).
43. M. Yaylaci and M. Avcar, "Finite element modeling of contact between an elastic layer and two elastic quarter planes," Int. J. Computers and Concrete, **26**, No 2, 107-114 (2020).
44. M. Yaylaci, G. Adiyaman, E. Öner and A. Birinci, "Examination of analytical and finite element solutions regarding contact of a functionally graded layer," Structural Engineering and Mechanics, **76**, No. 3, 325-336 (2020).
45. E. Öner, M. Yaylaci, and A. Birinci, "Analytical solution of a contact problem and comparison with the results from FEM," Structur. Eng. and Mech., **54**, No. 4, 607-622 (2015).

46. M. Pourabdy, M. Shishesaz, S. Shahrooi, S. Alireza. And S. Roknizadeh, "Analysis of axisymmetric vibration of functionally-graded circular nano-plate based on the integral form of the strain gradient model," J. Appl. and Comput. Mech., **7**, No. 4, 2196- 2220 (2015).
47. A. A. Daikh, M. S. A. Houari, and M. A. Eltaher, "A novel nonlocal strain gradient Quasi-3D bending analysis of sigmoid functionally graded sandwich nanoplates," Compos. Struct., **262**, 113347 (2021).
48. A. Bouhadra, A. Menasria, and M. Ali Rachedi, "Boundary conditions effect for buckling analysis of porous functionally graded nanobeam," Adv. Nano Research, **10**, No. 4, 313-325 (2021).
49. S. Srinivas, C. J. Rao, and A. K. Rao, "An exact analysis for vibration of simply-supported homogeneous and laminated thick rectangular plates," J. Sound and Vibration, **12**, No. 2, 187-199 (1970).
50. J. M. Whitney and N. J. Pagano. "Shear deformation in heterogeneous anisotropic plates," J. Appl. Mech., **37**, 1031-1036 (1070).
51. S. Yin, T. Yu, and P. Liu, "Free vibration analyses of FGM thin plates by isogeometric analysis based on classical plate theory and physical neutral surface," Adv. in Mech. Eng., **5**, 634584 (2013).
52. Q. LI, V. P. IU, and K. P. KOU, "Three-dimensional vibration analysis of functionally graded material sandwich plates," J. Sound and Vibration, **311**, No. 1-2, 498-515 (2008).